

Multi-Modal Representation Learning via Semi-Supervised Rate Reduction for Generalized Category Discovery

Wei He¹, Xianghan Meng¹, Zhiyuan Huang¹, Xianbiao Qi², Rong Xiao², Chun-Guang Li^{*,1}

¹ School of Artificial Intelligence, Beijing University of Posts and Telecommunications

{wei.he, huangzhiyuan, mengxianghan, lichunguang}@bupt.edu.cn

² Intellifusion Inc., Shenzhen, P.R. China

Abstract

Generalized Category Discovery (GCD) aims to identify both known and unknown categories, with only partial labels given for the known categories, posing a challenging open-set recognition problem. State-of-the-art approaches for GCD are usually built on multi-modality representation learning, which pays heavily attention to inter-modality alignment rather than intra-modality alignment. In this paper, we propose a novel and effective multi-modal representation learning approach for GCD via Semi-Supervised Rate Reduction, called SSR²-GCD, to learn cross-modality representations with desired underlying structures via properly harnessing intra-modality alignment. Moreover, to boost knowledge transfer, we integrate the information from prompt candidates by leveraging the inter-modal alignment offered by Vision Language Models. We conduct extensive experiments on generic and fine-grained benchmark datasets, demonstrating superior performance of the proposed approach and verifying the importance of intra-modality alignment. The code is available at: <https://github.com/hewei98/SSR2-GCD>.

1. Introduction

Generalized Category Discovery (GCD) has emerged as a natural and challenging extension of open-set recognition with the aim of discovering categories (i.e., patterns) in the open world [20, 22]. The goal of GCD is to recognize both known and unknown categories, going beyond the standard open-set recognition problem by leveraging knowledge learned from known categories to discover unknown categories. For example, in the typical setting of GCD task, half of categories are partially labeled (known) and the rest of categories remain unlabeled (unknown). Such a setting

is relevant to real-world exploration scenarios in which data exhibit a mixture of known and unknown categories.

Roughly speaking, existing state-of-the-art approaches to address GCD problem follow a two-phase framework: a) generating representations for images by fine-tuning the pre-trained models, and b) applying clustering algorithms on the learned representations of all unlabeled data. However, the representations derived from a single visual modality may lack sufficient discriminative information, especially when discovering visually similar categories.

For human being, it is consciously or unconsciously leveraging information or cues from multiple modalities to recognize unknown categories. Recently, there are a few attempts to explore multi-modal frameworks for GCD in image modality by integrating information from textual modality. For example, CLIP-GCD [16] leverages a knowledge database to search for similar texts of query images; TextGCD [32] constructs prompts from tag and attribute lexicons; and GET [24] learns a textual inversion network to generate prompts. These frameworks for multi-modal GCD have exploited textual cues into visual datasets to perform inter-modality alignment for cross-modality representation learning, but still lack sufficient consideration on the underlying structure of the distribution in the learned representation. For example, an existing CLIP-style inter-modality loss [18] or a GCD-style intra-modality loss [22] is incorporated to conduct inter-modality alignment for representation learning, lacking of a proper loss to harness intra-modality alignment. Thus the insights into the interactions between inter-modality alignment and intra-modality alignment in multi-modal representation learning are still vague.

In this paper, we attempt to incorporate the maximal coding rate reduction principle [28] into multi-modal representation learning for GCD, and present a novel and efficient approach, called Semi-Supervised Rate Reduction (SSR²-GCD). Specifically, in SSR²-GCD, a so-called SSR² loss, which encourages intra-modal consistency, is employed to learn desired structured representations. Unlike the existing multi-modal GCD approaches, in SSR²-GCD, the

* Chun-Guang Li is the corresponding author.

learned cross-modality representations for both known and unknown categories are compressed in a balanced manner. Moreover, we also present a Retrieval-based Text Aggregation (RTA) strategy to enhance the text generation, in which the information from augmented prompt candidates is aggregated to generate semantic-rich textual representations.

Paper Contributions. The contributions of the paper are highlighted as follows.

- We propose a Semi-Supervised Rate Reduction framework for GCD (SSR²-GCD) to learn structured representations with desired distribution structures.
- We present an effective Retrieval-based Text Aggregation (RTA) strategy for generating semantic-rich representations to boost knowledge transfer.
- We conduct extensive experiments, showing superior performance of the proposed approach and validating the importance of intra-modality alignment.

2. Relate Work

Generalized Category Discovery. GCD considers a realistic scenario in which the unlabeled dataset includes samples from both known and unknown categories, requiring simultaneous discovering of known and unknown categories. Initially, Vaze et al. [22] leverage supervised and self-supervised contrastive learning to refine the features produced by pre-trained vision models and use k -means [1, 13] algorithms for clustering. Then, SimGCD [27] introduces a parametric classifier to replace the non-parametric clustering and incorporates an entropy regularization to alleviate the degradation of classifier on unknown categories; SelEx [19] leverages a hierarchical semi-supervised k -means and achieves better results on fine-grained datasets; GPC [31] employs a mixture of Gaussian models to learn representations while estimating the number of unknown categories; PromptCAL [30] introduces a contrastive affinity learning framework, in which auxiliary visual prompts are incorporated to address the false negative-induced category collision issue; HypCD [12] considers both hyperbolic distance and angle between samples to learn hierarchy-aware representations. However, all these approaches mentioned above exploit the visual cues only.

Multi-modal Generalized Category Discovery. Existing Multi-modal GCD methods usually leverage the external guidance of textual modality brought by Vision-language pre-trained models (VLMs) to facilitate knowledge transfer between known and unknown categories. For instance, CLIP-GCD [16] leverages a knowledge database to generate texture descriptions and concatenates both the visual embedding and text embedding obtained from a frozen CLIP backbone for clustering; TextGCD [32] proposes a retrieval-based text generation method to generate semantic-rich texture descriptions by incorporating abundant tag and attribute candidates and introduces a co-

teaching technique to align the clustering outputs of vision and text branches. However, TextGCD simply employs the inter-modal contrastive loss of CLIP to fine-tune the backbone and uses the similarities within each modality for intra-modal clustering. Recently, GET [24] trains a textual inversion network [3] that maps the image embedding to pseudo textual token for unlabeled images. In the GCD setting, however, only class names of known categories are available preventing the textual inversion network from generating high-quality pseudo-tokens for images belonging to unknown categories. Although these methods achieve promising results, the interaction between inter-modal alignment and intra-modal alignment is unclear yet.

3. Preliminaries

3.1. Problem Notation

Denote data set as $\mathcal{D}_L \cup \mathcal{D}_U$, consisting of labeled data $\mathcal{D}_L = (\mathbf{x}_i, y_i^l)_{i=1}^M \subseteq \mathcal{X} \times \mathcal{Y}_L$ and unlabeled data $\mathcal{D}_U = (\mathbf{x}_i, y_i^u)_{i=1}^N \subseteq \mathcal{X} \times \mathcal{Y}_U$, where \mathcal{Y}_L and \mathcal{Y}_U denote the label sets and $\mathcal{Y}_L \subset \mathcal{Y}_U$. In GCD setting, the labeled samples in \mathcal{D}_L are from the known categories; whereas unlabeled samples in \mathcal{D}_U are either from the known categories or from some unknown categories. As usual, the total number of categories $K = |\mathcal{Y}_U|$ is given (or can be estimated). The goal of GCD is to estimate the labels of samples in \mathcal{D}_U .

3.2. Multi-modal GCD Pipelines

The common multi-modal GCD pipelines consist of three components: a) text generation, b) representation learning and c) clustering.

Text Generation. To introduce textual cues, pre-trained VLMs are usually leveraged to generate pseudo-texts for query images, in which retrieval-based methods [11, 32] are used to construct a prompt set \mathcal{P} and search for the suitable prompt $p \in \mathcal{P}$ for the query image. For instance, TextGCD [32] uses the category name in ImageNet [6] to construct a tag lexicon and leverages GPT3 [4] to generate attributes for these tags, in which the tags and attributes are used to construct the prompt for each query image.

Representation Learning. Given query images and their corresponding pseudo-texts, multi-modal GCD frameworks usually further refine the representations. For instance, TextGCD [32] learns the representations by simply using a CLIP-style inter-modal contrastive loss

$$\mathcal{L}_{\text{CLIP}} = -\frac{1}{|B|} \sum_{i \in B} \log \frac{\exp(\mathbf{z}_i^{\text{I}\top} \mathbf{z}_i^{\text{T}} / \tau_c)}{\sum_{j \neq i} \exp(\mathbf{z}_i^{\text{I}\top} \mathbf{z}_j^{\text{T}} / \tau_c)}, \quad (1)$$

where B denotes the mini-batch of data, $\mathbf{z}_i^{\text{I}}, \mathbf{z}_i^{\text{T}} \in \mathbb{R}^d$ denote the embeddings of the i -th image and pseudo-text, and

τ_c is the temperature factor. Minimizing $\mathcal{L}_{\text{CLIP}}$ encourages the inter-modal alignment between image and text, but does not account for intra-modal alignment within each modality. GET [24] encourages the inter-modal alignment in representation learning, while incorporating the following supervised and unsupervised contrastive losses

$$\mathcal{L}_{\text{con}} = \lambda \mathcal{L}_{\text{con}}^s + (1 - \lambda) \mathcal{L}_{\text{con}}^u, \quad (2)$$

$$\mathcal{L}_{\text{con}}^s = - \sum_{i \in B_\ell} \frac{1}{|\mathcal{N}_i|} \sum_{j \in \mathcal{N}_i} \log \frac{\exp(\mathbf{z}_i^\top \mathbf{z}'_j / \tau_a)}{\sum_{m \neq i} \exp(\mathbf{z}_i^\top \mathbf{z}'_m / \tau_a)},$$

$$\mathcal{L}_{\text{con}}^u = - \sum_{i \in B} \log \frac{\exp(\mathbf{z}_i^\top \mathbf{z}'_i / \tau_b)}{\sum_{m \neq i} \exp(\mathbf{z}_i^\top \mathbf{z}'_m / \tau_b)},$$

to encourage the intra-modal alignment, where λ is the balancing parameter, B_ℓ denotes the labeled subset of B , \mathbf{z}_i and \mathbf{z}'_i are embeddings of augmented data pairs, \mathcal{N}_i is the index set of samples with the same label as the i -th sample, and τ_a and τ_b are the temperature parameters. Still, the intra-modal representation learning in multi-modal GCD frameworks adheres to the paradigm of uni-modal counterparts, and fails to resolve its inherent issue, i.e., minimizing \mathcal{L}_{con} results in an *imbalanced compression* of embeddings, because $\mathcal{L}_{\text{con}}^u$ pulls positive augmented data pairs across all categories, whereas $\mathcal{L}_{\text{con}}^s$ further pulls labeled data only for known categories. As illustrated in Figure 1, such an imbalanced compression issue prevents clustering algorithms from identifying clusters accurately.

Clustering. Existing multi-modal GCD frameworks usually follow SimGCD [27] to cluster unlabeled data via integrating a cross-entropy loss [9], a self-distillation loss [2] and an entropy regularizer, i.e.,

$$\mathcal{L}_{\text{cls}} = \sum_{i \in B_\ell} \ell_{\text{CE}}(\mathbf{y}_i^*, \mathbf{y}_i) + \gamma \sum_{i \in B} \ell_{\text{CE}}(\mathbf{y}'_i, \mathbf{y}_i) - \mu H(\bar{\mathbf{y}}), \quad (3)$$

where γ and μ are the balancing parameters, ℓ_{CE} denotes the cross-entropy loss, \mathbf{y}_i^* is the ground-truth label of the i -th image, \mathbf{y}_i is the prediction of the i -th embedding \mathbf{z}_i , \mathbf{y}'_i is the prediction of the augmented counterpart \mathbf{z}'_i with a sharper temperature in softmax , and an entropy regularizer $H(\bar{\mathbf{y}}) = - \sum_k \bar{\mathbf{y}}^{(k)} \log \bar{\mathbf{y}}^{(k)}$ is used to prevent degenerated predictions in new classes, in which $\bar{\mathbf{y}} = \frac{1}{2|B|} \sum_{i \in B} (\mathbf{y}_i + \mathbf{y}'_i)$ denotes the mean prediction of $\mathbf{y}_i + \mathbf{y}'_i$ in a mini-batch using the same temperature, and $\bar{\mathbf{y}}^{(k)}$ is the entry of $\bar{\mathbf{y}}$ associating to the k -th class. For example, GET trains an MLP by the loss in Eq. (3) to produce predictions for both image and text embeddings, whereas TextGCD implements dual-branch classifiers to handle image and text embeddings, respectively, and use high confidence samples to supervise the classifier training via a co-teaching loss

$$\mathcal{L}_{\text{co-teach}} = \sum_{i \in \mathcal{S}^I} \ell_{\text{CE}}(\mathbf{y}_i^I, \mathbf{y}_i^T) + \sum_{j \in \mathcal{S}^T} \ell_{\text{CE}}(\mathbf{y}_j^T, \mathbf{y}_j^I), \quad (4)$$

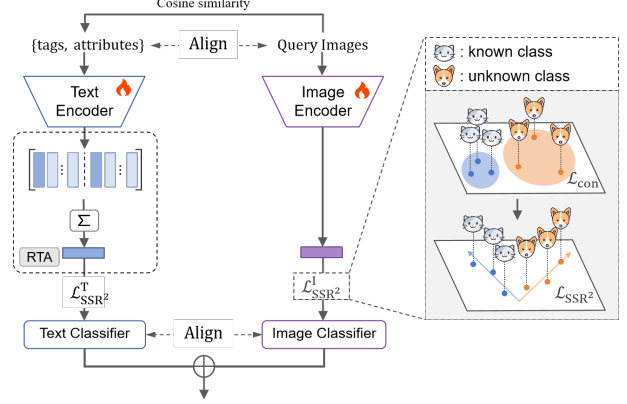


Figure 1. Illustration of our proposed framework: SSR^2 -GCD.

where \mathcal{S}^I and \mathcal{S}^T are the sample sets selected based on the confidence score of \mathbf{y}^I and \mathbf{y}^T , respectively.

4. Our Proposed Approach: SSR^2 -GCD

Our SSR^2 -GCD consists of three of modules: a) Retrieval-based Text Aggregation (RTA) module for text generation and aggregation; b) Semi-Supervised Rate Reduction (SSR^2) module for representation learning; and c) dual-branch classifiers to learn pseudo-labels. For clarity, we illustrate our proposed framework in Figure 1.

4.1. Retrieval-based Text Aggregation

Since that incorporating more information from multiple tag and attribute candidates is helpful to discover the unknown categories, we follow TextGCD [32] for text generation, i.e., constructing tag and attribute lexicons and then searching for similar tags and attributes. However, the way to construct prompts in TextGCD is sub-optimal because that CLIP fails to generate satisfactory embeddings for prompts exceeding 20 tokens due to its limitation in handling long textual prompts [29]. Given CLIP text encoder \mathcal{F}^T and tokenizer \mathcal{T} , instead, in this paper, we use the text encoder \mathcal{F}^T to embed the prompts of the top- c most similar tag and attribute and compute the textual embedding by:

$$\mathbf{z}^T = \sum_{i=1}^c \sigma_i [\mathcal{F}^T(\mathcal{T}(a_i)) + \mathcal{F}^T(\mathcal{T}(b_i))], \quad (5)$$

where a_i and b_i are the i -th most similar tag and attribute of the query image, respectively, as ranked by the cosine similarity between their embeddings, and σ_i is defined as

$$\sigma_i = \begin{cases} 1 - \alpha & \text{if } i = 1 \\ \frac{\alpha}{c-1} & \text{otherwise,} \end{cases} \quad (6)$$

which is used to assign higher weights to the most similar tag and attribute and aggregate information from other candidates, where $\alpha > 0$ is hyper-parameter (e.g., $\alpha = 0.5$).

Such a strategy allows us to aggregate richer information from a larger set of candidates (e.g., $c = 4$).

4.2. Semi-Supervised Rate Reduction Module for Representation Learning

To learn structured representations from intra-modal relationships and achieve balanced compression across both known and unknown categories, we propose a **Semi-Supervised Rate Reduction (SSR²)** approach, which employs a SSR² objective as follows:

$$\mathcal{L}_{\text{SSR}^2} = -R(\mathbf{Z}) + R_c^s(\mathbf{Z}, \mathbf{Y}^*) + R_c^u(\mathbf{Z}, \mathbf{Y}), \quad (7)$$

where

$$\begin{aligned} R(\mathbf{Z}) &= \log \det \left(\mathbf{I} + \frac{d}{N\epsilon^2} \mathbf{Z}\mathbf{Z}^\top \right), \\ R_c^s(\mathbf{Z}_s, \mathbf{Y}^*) &= \sum_{j=1}^k \frac{N_j^s}{N} \log \det \left(\mathbf{I} + \frac{d}{N_j^s \epsilon^2} \mathbf{Z}_s \text{Diag}(\mathbf{Y}_j^*) \mathbf{Z}_s^\top \right), \\ R_c^u(\mathbf{Z}_u, \mathbf{Y}) &= \sum_{j=1}^k \frac{N_j^u}{N} \log \det \left(\mathbf{I} + \frac{d}{N_j^u \epsilon^2} \mathbf{Z}_u \text{Diag}(\mathbf{Y}_j) \mathbf{Z}_u^\top \right), \end{aligned}$$

where \mathbf{Z} is the embeddings of a mini-batch, $\mathbf{Z}_s, \mathbf{Z}_u$ are the embeddings of labeled and unlabeled data, \mathbf{Y}^* is the ground-truth labels, \mathbf{Y} is the pseudo-labels predicted by classifiers, \mathbf{I} is the identity matrix, k is the number of categories, $\epsilon > 0$ is the hyper-parameter, N_j^s is the number of labeled data points assigned by \mathbf{Y}^* that belong to the j -th class, and N_j^u is the number of unlabeled data points assigned by \mathbf{Y} that belong to the j -th class.

Specifically, during training we fine-tune the image and text encoders of CLIP [18] with the associated loss, that is to replace the embedding \mathbf{Z} and the pseudo-labels \mathbf{Y} by the image and text embeddings $\{\mathbf{Z}^I, \mathbf{Z}^T\}$ and the pseudo-labels of dual-branch classifiers $\{\mathbf{Y}^I, \mathbf{Y}^T\}$, respectively, i.e.,

$$\begin{aligned} \mathcal{L}_{\text{SSR}^2}^I &= -R(\mathbf{Z}^I) + R_c^s(\mathbf{Z}^I, \mathbf{Y}^*) + R_c^u(\mathbf{Z}^I, \mathbf{Y}^I), \\ \mathcal{L}_{\text{SSR}^2}^T &= -R(\mathbf{Z}^T) + R_c^s(\mathbf{Z}^T, \mathbf{Y}^*) + R_c^u(\mathbf{Z}^T, \mathbf{Y}^T). \end{aligned} \quad (8)$$

Remarks 1. Our SSR² is inspired by the structured representation learning principle—Maximal Coding Rate Reduction [28], which is developed for supervised settings. The effects of introducing SSR² are twofold. First, maximizing the term $R(\cdot)$ in Eq. (7) expands the entire embeddings, whereas minimizing the terms $R_c^s(\cdot)$ and $R_c^u(\cdot)$ encourages the embeddings of each category to span low-dimensional subspaces with balanced matrix ranks, as proved in [26, 28]. Owing to such a desired property, the representations of both known and unknown categories are **compressed in balanced manner**. To our knowledge, this is the first work to address the imbalanced compression issue in contrastive-based representation learning for GCD. Second, we found

in experiments that the inter-modal alignment leads to **intra-modal misalignment**; whereas our SSR² emphasizes on aligning intra-modal relationships while tolerating the discrepancies between modalities.

4.3. Training Strategy

To fully discover the differences between modalities, we deploy dual-branch classifiers to separately tackle with image and text embeddings, which are trained concurrently with the representation learning. Specifically, the procedure to train our SSR²-GCD consists of the following two stages.

Warm-up Stage. To prevent erroneous guidance of representation learning induced by pseudo-labels from untrained classifiers, the self-supervised term $R_c^u(\mathbf{Z}, \mathbf{Y})$ in Eq. (7) is excluded in the early training phase, i.e., $\mathcal{L}_{\text{SSR}^2}$ reduces to

$$\mathcal{L}_{\text{SSR}^2\text{-sup}} = -R(\mathbf{Z}) + R_c^s(\mathbf{Z}, \mathbf{Y}^*). \quad (9)$$

To train the classifiers, the loss \mathcal{L}_{cls} in Eq. (3) is adopted. Thus the objective in the warm-up stage is:

$$\mathcal{L}_{\text{warm}} = \mathcal{L}_{\text{SSR}^2\text{-sup}}^I + \mathcal{L}_{\text{SSR}^2\text{-sup}}^T + \mathcal{L}_{\text{cls}}^I + \mathcal{L}_{\text{cls}}^T, \quad (10)$$

where the superscripts ^I and ^T denote the losses applied to visual and textual modalities, respectively.

Alignment Stage. To align the orders of pseudo-labels predicted by dual-branch classifiers, we follow the co-teaching strategy in TextGCD [32]. Thus by combining the co-teaching loss $\mathcal{L}_{\text{co-teach}}$ in Eq (4), the total training loss in the alignment stage is:

$$\mathcal{L}_{\text{align}} = \mathcal{L}_{\text{SSR}^2}^I + \mathcal{L}_{\text{SSR}^2}^T + \mathcal{L}_{\text{cls}}^I + \mathcal{L}_{\text{cls}}^T + \mathcal{L}_{\text{co-teach}}. \quad (11)$$

After training, the predicted pseudo-label of the i -th image is determined by $\text{argmax}(\mathbf{y}_i^I + \mathbf{y}_i^T)$.

Remarks 2. The clustering algorithm of our framework is the same as that in TextGCD [32]. However, the key difference lies in representation learning. Specifically, TextGCD emphasizes only on the inter-modal alignment without incorporating the intra-modal constraints, and the learning of the two classifiers is based on intra-modal similarities. As pointed out in [14], using inter-modal alignment loss without intra-modal constraint will lead to intra-modal misalignment, i.e., the intra-modal similarities might not correspond to the actual pair-wise relationships, thereby degrading the clustering performance. In contrast, in our SSR²-GCD, the intra-modal relationships are well aligned by using $\mathcal{L}_{\text{SSR}^2}$, and thus the two classifiers produce satisfactory results. In addition, the predictions produced by the dual-branch classifiers are also used as self-supervised signals to guide the joint representation learning, as shown in Eq. (7).

5. Experiments

To validate the effectiveness of our proposed approach, we conduct extensive experiments on eight benchmark datasets and also provide in-depth evaluation and ablation studies.

Table 1. The average ACC (%) on ImageNet datasets. “†” denotes the reproduced results using CLIP backbone.

Method	ImageNet-100			ImageNet-1k			
	All	Old	New	All	Old	New	
<i>DINOv1</i>	GCD	74.1	89.8	66.3	52.5	72.5	42.2
	SimGCD	83.0	93.1	77.9	57.1	77.3	46.9
	SPTNet	85.4	93.2	81.4	-	-	-
	SelEx	83.1	93.6	77.8	-	-	-
	Hyp-SelEx	86.8	94.6	82.8	-	-	-
<i>CLIP</i>	SimGCD†	86.1	94.5	81.9	48.2	72.7	36.0
	CLIP-GCD	84.0	95.5	78.2	-	-	-
	TextGCD	88.0	92.4	85.2	64.8	77.8	58.3
	GET	91.7	95.7	89.7	62.4	74.0	56.6
	Ours	92.1	96.0	90.2	66.7	77.3	61.1

Datasets. We evaluate the performance of GCD methods on four generic datasets, i.e., CIFAR-10/-100 [8], and ImageNet-100/-1k [6], and four fine-grained datasets, i.e., CUB-200-2011 [23], Stanford Cars [7], Oxford Pets [17] and Flowers102 [15]. Following the GCD protocol [22], half of the samples from the known categories are selected to form the labeled dataset \mathcal{D}_L , while the remaining samples are to form the unlabeled dataset \mathcal{D}_U .

Metrics. Given the ground-truths of \mathcal{D}_U , one can compute the clustering accuracy (ACC) using Hungarian matching algorithm [10]. Following the GCD protocol [22], we report ACC on all categories (“All”), on known categories (“Old”), and on unknown categories (“New”), respectively. The average ACC over 3 trials is reported.

Implementation Details. In Retrieval-based Text Aggregation, we use CLIP-H/14 [18] to search prompt candidates to ensure a fair comparison to TextGCD [32]. During training, we use CLIP-B/16 encoders to produce text and image features. We report the performance of uni-modal counterparts using DINO [5] with ViT-B/16. The classifier parameters are set with the default configurations of SimGCD [27] and TextGCD [32]. We use $\epsilon = 0.5$ in our SSR²-GCD.

5.1. Performance on Benchmark Datasets

We compare the performance of our SSR²-GCD to uni-modal GCD methods, including GCD [22], GPC [31], SimGCD [27], PromptCAL [30], SPTNet [25], SelEx [19] and HypCD [12] with the SelEx backbone (denoted by “Hyp-SelEx”), and multi-modal GCD methods, including CLIP-GCD [16], TextGCD [32] and GET [24]. Since that GET did not provide the results on Oxford Pets and Flowers102, we reproduced the results with the open-source code. Experimental results are listed in Tables 1 and 2. As can be read, our SSR²-GCD consistently outperforms all other multi-modal counterparts on all test datasets. We can also observe that our SSR²-GCD narrows the accuracy gap between “Old” and “New” categories. HypCD

achieves the highest accuracy on CUB when using SelEx as the backbone, in which the embedding space is changed from Euclidean to hyperbolic, and thus it is complementary to our SSR²-GCD. In addition, our SSR²-GCD excels notably on Stanford Cars and Flowers102, achieving accuracy of 89.2% and 93.5% on “All” categories, outperforming all other baselines by 3.1% and 6.3%, respectively. Note that CLIP performs poorly in out-of-domain datasets including Flowers102, achieving an accuracy of 70.4% in zero-shot classification [18], whereas our SSR²-GCD effectively refines the representations generated by CLIP to the target domain of Flowers102 and yields satisfactory performance.

5.2. Evaluation on Representation Learning

Alignment: Inter-Modal vs. Intra-Modal. To evaluate the effect of using inter-modal and intra-modal alignments in our framework, we keep the text generation and classification methods the same and report the performance of using different losses for representation learning, including inter-modal loss (i.e., $\mathcal{L}_{\text{CLIP}}$ in Eq. (1)), intra-modal losses (i.e., \mathcal{L}_{con} in Eq. (2) and our $\mathcal{L}_{\text{SSR}^2}$ in Eq. (7)) and their combinations (e.g., $\mathcal{L}_{\text{CLIP}} + \mathcal{L}_{\text{con}}$). The experimental results are listed in Table 3. We found that encouraging inter-modal alignment alone provides merely limited performance gain when compared to using the intra-modal losses alone, since that the learning of classifiers is based on the intra-modal relationships within each modality. Specifically, our framework achieves the highest accuracy on five benchmark datasets when using the proposed $\mathcal{L}_{\text{SSR}^2}$. Our framework trained with supervised and unsupervised contrastive loss \mathcal{L}_{con} is still a strong intra-modal learning baseline, achieving the highest accuracy on CIFAR-100. Interestingly, combining $\mathcal{L}_{\text{CLIP}}$ with intra-modal loss \mathcal{L}_{con} or $\mathcal{L}_{\text{SSR}^2}$ cannot significantly improve the clustering accuracy and may even degrade it. Note that \mathcal{L}_{con} outperforms $\mathcal{L}_{\text{CLIP}} + \mathcal{L}_{\text{con}}$ on four datasets, except for CUB and Oxford Pets; whereas $\mathcal{L}_{\text{SSR}^2}$ surpasses $\mathcal{L}_{\text{CLIP}} + \mathcal{L}_{\text{SSR}^2}$ on all datasets, suggesting that explicitly imposing inter-modal alignment could deteriorate the intra-modal alignment.

SSR² Works Well for Inter-modal Alignment and Intra-modal Alignment. To evaluate the role of the SSR² objective in inter-modal and intra-modal alignments, we conduct a set of experiments to report the distributions of the pairwise similarity calculated from image-text, image-image, and text-text pairs, when using the loss $\mathcal{L}_{\text{SSR}^2}$ or $\mathcal{L}_{\text{CLIP}}$ at the beginning of the training (i.e., epoch 0), at the end of the warm-up (i.e., epoch 10) and at the end of the training (i.e., epoch 200), respectively. Experimental results are shown in Figure 2. Clearly, we observe that the distributions of inter-modal similarities and intra-modal similarities exhibit substantial divergence at the beginning, where the distributions of image-image and text-text similarities within each modality also differ notably. When using the proposed loss

Table 2. The average ACC (%) on generic and fine-grained datasets. “†” denotes the reproduction of using CLIP backbone.

Method	CIFAR-10			CIFAR-100			CUB			Stanford Cars			Oxford Pets			Flowers102		
	All	Old	New	All	Old	New	All	Old	New	All	Old	New	All	Old	New	All	Old	New
GCD	91.5	97.9	88.2	73.0	76.2	66.5	51.3	56.6	48.7	39.0	57.6	29.9	80.2	85.1	77.6	74.4	74.9	74.1
GPC	92.2	98.2	89.1	77.9	85.0	63.0	55.4	58.2	53.1	42.8	59.2	32.8	-	-	-	-	-	-
SimGCD	97.1	95.1	98.1	80.1	81.2	77.8	60.3	65.6	57.7	53.8	71.9	45.0	87.7	85.9	88.6	71.3	80.9	66.5
PromptCAL	97.9	96.6	98.5	81.2	84.2	75.3	62.9	64.4	62.1	50.2	70.1	40.6	-	-	-	-	-	-
SPTNet	97.3	95.0	98.6	81.3	84.3	75.6	65.8	68.8	65.1	59.0	79.2	49.3	-	-	-	-	-	-
SelEx	95.9	98.1	94.8	82.3	85.3	76.3	73.6	75.3	72.8	58.5	75.6	50.3	92.5	91.9	92.8	-	-	-
Hyp-SelEx	96.7	97.6	96.3	82.4	85.1	77.0	79.8	75.8	81.8	62.9	80.0	54.7	-	-	-	-	-	-
SimGCD†	96.6	94.7	97.5	81.6	82.6	79.5	62.0	76.8	54.6	75.9	81.4	73.1	88.6	75.2	95.7	75.3	87.8	69.0
CLIP-GCD	96.6	97.2	96.4	85.2	85.0	85.6	-	-	-	62.8	77.1	55.7	70.6	88.2	62.2	76.3	88.6	70.2
TextGCD	98.2	98.0	98.6	85.7	86.3	84.6	76.6	80.6	74.7	86.1	91.8	83.9	93.7	93.2	94.0	87.2	90.7	85.4
GET	97.2	94.6	98.5	82.1	85.5	75.5	77.0	78.1	76.4	78.5	86.8	74.5	91.1	89.7	92.4	85.5	90.8	81.3
Ours	98.5	98.3	98.6	86.4	86.2	86.9	78.3	78.5	78.2	89.2	93.1	87.3	95.7	95.1	96.0	93.5	93.3	93.9

Table 3. Evaluation of different representation learning methods. Average ACC (%) on “All” categories is reported. “N/A”: frozen CLIP.

Rep. Losses	Inter	Intra	CIFAR-10	CIFAR-100	CUB	Stanford Cars	Oxford Pets	Flowers102
N/A	×	×	97.9	84.1	74.5	86.0	91.9	87.4
$\mathcal{L}_{\text{CLIP}}$	✓	×	98.3	86.0	76.7	87.0	94.1	89.7
\mathcal{L}_{con}	×	✓	<u>98.4</u>	86.7	77.5	87.9	94.9	91.8
$\mathcal{L}_{\text{SSR}^2}$	×	✓	98.5	<u>86.4</u>	78.3	89.2	95.7	93.5
$\mathcal{L}_{\text{CLIP}}+\mathcal{L}_{\text{con}}$	✓	✓	98.2	86.3	<u>78.0</u>	86.7	95.0	90.9
$\mathcal{L}_{\text{CLIP}}+\mathcal{L}_{\text{SSR}^2}$	✓	✓	98.3	86.1	<u>77.2</u>	<u>88.1</u>	<u>95.0</u>	<u>92.9</u>

$\mathcal{L}_{\text{SSR}^2}$, the distributions of intra-modal similarities are well aligned in the warm-up stage, and all distributions gaps almost vanish at the end of the training. Specifically, optimizing the intra-modal alignment loss (i.e., $\mathcal{L}_{\text{SSR}^2}$) alone still helps to align the distributions of image-text similarities. When using $\mathcal{L}_{\text{CLIP}}$, although the distributions of image-text similarities are aligned well, the image-image and text-text similarities, which are critical for GCD, are poorly aligned.

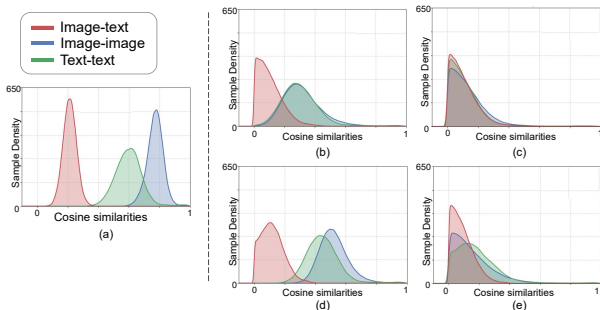


Figure 2. Distributions of pairwise similarities on Flowers102. (a): at the beginning of training. (b)-(c): training with $\mathcal{L}_{\text{SSR}^2}$ at epochs 10 and 200. (d)-(e): training with $\mathcal{L}_{\text{CLIP}}$ at epochs 10 and 200.

Evaluation on Intra-modal Alignment Behaviors. For the reason why the intra-modal alignment loss works well in multi-modal representation learning, we account it in the implicit inter-modal alignment and the implicit hypoth-

esis of clustering algorithms. On one hand, the initial textual and visual representations are well aligned by using a pretrained CLIP backbone to select similar pseudo text-image pairs, and thus further encouraging inter-modal alignment between the embeddings of images and pseudo texts could be detrimental. By contrast, minimizing the proposed $\mathcal{L}_{\text{SSR}^2}$ objective does not compromise the inter-modal alignment; as shown in Figure 2, it implicitly promotes such an alignment. On the other hand, most GCD frameworks, including our $\text{SSR}^2\text{-GCD}$, employs the self-distillation loss for clustering. As shown in Eq. (3), the self-distillation loss minimizes the cross-entropy between the predictions of the augmented data pairs from the same modality, involving only the consistency of the intra-modal embedding pairs. In other words, using the loss in Eq. (3) is built on the assumption that the intra-modal embeddings of augmented data pairs should be close enough to be assigned to the same cluster. To quantify the intra-modal consistency, we construct the adjacency matrices \mathbf{W} for each modality where $W_{i,j} = z_i^\top z_j$. Given the ground-truth categories $\{\mathcal{C}_1, \dots, \mathcal{C}_k\}$ indicated by their labels, one can quantify the consistency by computing the ratio of the weights on edges within each category to the weights on edges between different categories, i.e.,

$$\rho = \frac{1}{k} \sum_{\ell=1}^k \rho_\ell, \quad \rho_\ell = \frac{\sum_{i \in \mathcal{C}_\ell} \sum_{j \in \mathcal{C}_\ell} W_{i,j}}{\sum_{i \in \mathcal{C}_\ell} \sum_{j \notin \mathcal{C}_\ell} W_{i,j}}. \quad (12)$$

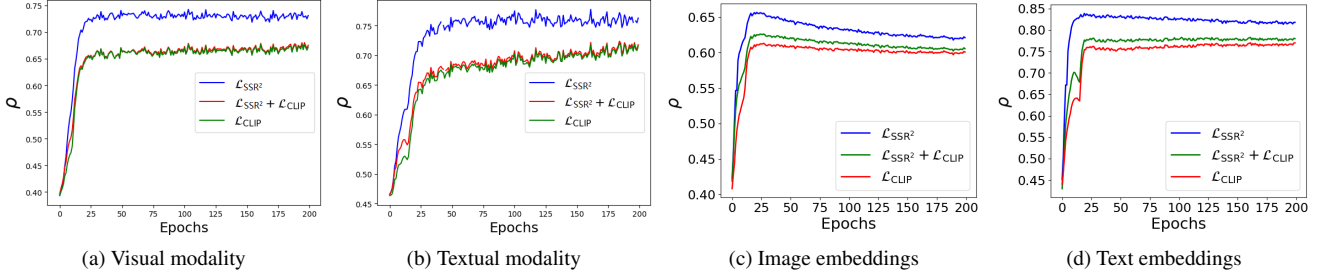


Figure 3. Consistency measure ρ as a function of training epoch when trained with different losses on different datasets. (a)-(b): on Flowers102. (c)-(d): on Stanford Cars.

Apparently, a larger value of ρ indicates a higher ratio of correct intra-category links to incorrect inter-category links, reflecting better consistency of intra-modal embeddings. We calculate the ratio ρ at different epochs during the training period when using different losses on Flowers102, and show it as a function of training epoch in Figure 3. As can be seen, using $\mathcal{L}_{\text{SSR}^2}$ achieves higher ρ than using $\mathcal{L}_{\text{CLIP}}$. While $\mathcal{L}_{\text{CLIP}}$ can implicitly enhance intra-class discriminability to some extent, it is insufficient to ensure intra-modal alignment and thus yields inferior clustering accuracy. This suggests that inter-modal alignment without any intra-modal constraint leads to intra-modal misalignment. Moreover, we observe that the ratio curve of using $\mathcal{L}_{\text{CLIP}} + \mathcal{L}_{\text{SSR}^2}$ rises in parallel with that of using $\mathcal{L}_{\text{SSR}^2}$ in the early training stages, but eventually converges to the curve of using $\mathcal{L}_{\text{CLIP}}$. This verifies that the inter-modal alignment may damage the learning of intra-modal consistency.

SSR² as a Compressor for Balanced Representation.

To evaluate the effectiveness of our $\mathcal{L}_{\text{SSR}^2}$, we conduct experiments to compare it to the widely used contrastive loss \mathcal{L}_{con} . To quantify the uniformity of the compression, we compute the numerical rank, which is defined as the number of leading singular values whose cumulative energy proportion reaches 95% of all singular values, of image embeddings per category, i.e., $\{\text{rank}(\mathbf{Z}^{(i)})\}_{i=1}^k$, where $\mathbf{Z}^{(i)}$ is the sub-matrix formed by the embeddings from the i -th ground-truth category. We train our framework via using \mathcal{L}_{con} and $\mathcal{L}_{\text{SSR}^2}$, respectively, compute the averaged ranks of “Old” categories and “New” categories, i.e., $\frac{1}{|\mathcal{Y}_L|} \sum_{i \in \mathcal{Y}_L} \text{rank}(\mathbf{Z}^{(i)})$ and $\frac{1}{(|\mathcal{Y}_U| \setminus |\mathcal{Y}_L|)} \sum_{j \in (\mathcal{Y}_U \setminus \mathcal{Y}_L)} \text{rank}(\mathbf{Z}^{(j)})$, on Flowers102 and Oxford Pets, and display the results in Figure 4. We can see that the average rank of the “Old” categories dramatically decreases during the training period when using the loss \mathcal{L}_{con} , which is much lower than that of the “New” categories. Intuitively, using the loss \mathcal{L}_{con} will overly compress the embeddings toward the contrastive prototypes of the known categories. In contrast, when training with the loss $\mathcal{L}_{\text{SSR}^2}$, the average ranks of the “Old” and the “New” categories are preserved well, avoiding collapse. To have a

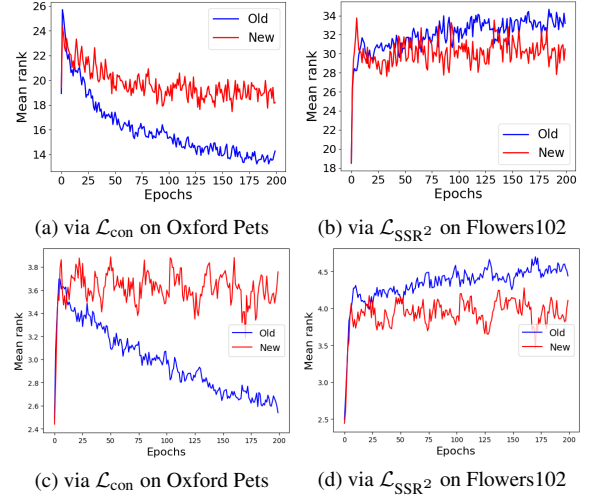


Figure 4. Mean ranks of image embeddings.

better intuition, we use t -SNE [21] to visualize the image embeddings from a frozen CLIP encoder, and trained via $\mathcal{L}_{\text{CLIP}}$, \mathcal{L}_{con} and our $\mathcal{L}_{\text{SSR}^2}$ on balanced dataset CIFAR-10. Experimental results are shown in Figure 5. We observe that our approach learns well-aligned representations that are uniformly distributed across categories and discriminative between categories. To evaluate the performance of SSR²-GCD on imbalanced datasets, we train our SSR²-GCD on *entire* Flowers102 (class-imbalanced) dataset and visualize the cosine similarity (ordered by ground-truths) and *effective ranks* of the learned features in Figure 6. As can be observed that, larger blocks (categories) tend to have higher ranks. This is because, the scaled compression term in the SSR² objectives tends to learn “balanced” embeddings, in which bigger categories span higher ranks with smaller singular values, smaller classes span lower ranks with larger singular values and the nonzero singular values within each class tend to be equal amplitude.

5.3. Ablation Study

To evaluate the effectiveness of each component in our SSR²-GCD, we conduct a set of experiments on Stanford Cars and Flowers-102, in which the baseline is set up by

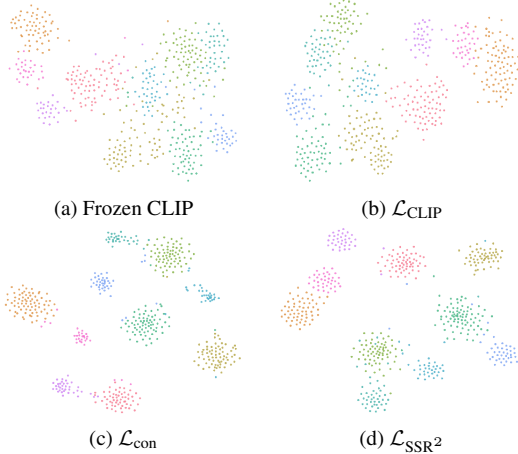


Figure 5. Visualizations of image embeddings.

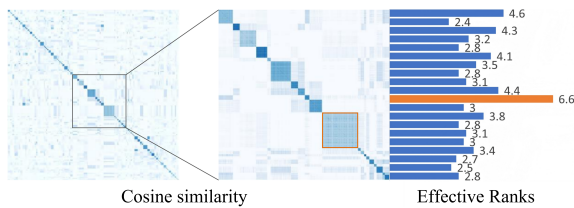


Figure 6. Cosine similarity (ordered by ground-truths) and cluster ranks on Flowers102.

using the most similar tag as pseudo-text, leveraging the frozen CLIP to generate the embeddings, and clustering both image and text embeddings via a single classifier with shared parameters. Experimental results are listed in Table 4. We can read that the co-taught dual-branch classifiers outperform the baseline by identifying disparities between modalities. The proposed RTA integrates richer information from tag and attribute candidates, thereby enhancing clustering performance on “New” categories. The intra-modal representation learning by using the loss \mathcal{L}_{SSR^2} is also critical, since the training of classifiers relies on well-aligned intra-modal consistency. Our SSR^2 -GCD achieves the best performance by integrating all the three components.

Table 4. Ablation study of different components.

Dual	RTA	\mathcal{L}_{SSR^2}	Stanford Cars			Flowers102		
			All	Old	New	All	Old	New
×	×	×	75.2	85.4	71.8	78.3	88.1	72.5
✓	×	×	81.7	90.3	77.1	83.9	88.3	81.3
✓	✓	×	86.0	91.0	83.4	87.4	90.8	85.5
✓	×	✓	85.5	91.7	82.2	89.1	91.8	88.0
✓	✓	✓	89.2	93.1	87.3	93.5	93.3	93.9

5.4. More Evaluations

Evaluation on RTA. In our proposed RTA, we introduce a hyper-parameter α to balance the use of the most-similar

Table 5. Effect of the hyper-parameter α in RTA strategy.

Data	α	0.2	0.3	0.4	0.5	0.6	0.7	0.8
CIFAR-10		98.3	98.4	98.4	98.5	98.3	98.2	97.8
CIFAR-100		86.0	86.6	86.7	86.4	85.8	85.2	84.1
Stanford Cars		87.1	88.7	88.9	89.2	88.8	87.2	86.4
Flowers102		92.9	93.3	93.3	93.5	92.8	92.1	91.5

candidates and other candidates. To evaluate the sensitivity to α , we report the accuracy of “All” categories on four generic and fine-grained datasets, with varying values of $\alpha \in \{0.2, 0.3, 0.4, 0.5, 0.6, 0.7, 0.8\}$ while keeping other components in our SSR^2 -GCD unchanged. As shown in Table 5, we observe that using the proposed RTA achieves the best performance on CIFAR-10, Stanford Cars and Flowers102 with $\alpha = 0.5$, and achieves the best performance on CIFAR-100 with $\alpha = 0.4$. Moreover, in RTA as shown in Eq.(5), we select multiple candidates for tags and attributes. To evaluate the effect of the number of candidates, we report the accuracy of “All” categories on CIFAR-10 and Stanford Cars, with varying number of tags and attributes in $\{1, 2, 3, 4, 5\}$, respectively. As shown in Figure 7, we can read that integrating more candidates yields consistent performance improvements. Specifically, the performance achieves the best when the number of tags and attributes is set to 3 or 4, respectively. More evaluations are provided in the Supporting Materials.

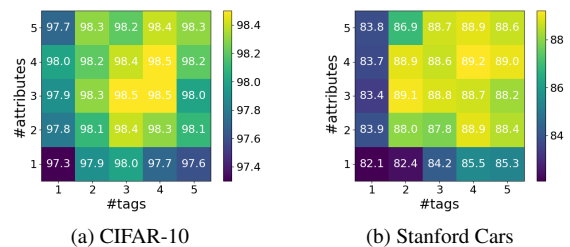


Figure 7. Effect of the number of candidates in RTA strategy.

6. Conclusion

We proposed a novel and effective multi-modal representation learning framework, called SSR^2 -GCD. To be specific, we incorporated a semi-supervised rate reduction loss to learn balanced structural representations for multi-modal GCD task. Moreover, we designed a retrieval-based text aggregation strategy to enhance text generation and thus boost knowledge transfer. We conducted extensive experiments on eight benchmark datasets, and experimental results demonstrated the effectiveness of our proposed SSR^2 -GCD approach and verified that prioritizing intra-modal consistency via SSR^2 is beneficial for multi-modal GCD.

Acknowledgments

This work is supported by the National Natural Science Foundation of China under Grant No. 62576048.

References

- [1] David Arthur and Sergei Vassilvitskii. k-means++: the advantages of careful seeding. In *Annual ACM-SIAM Symposium on Discrete Algorithms*, pages 1027–1035. SIAM, 2007. 2
- [2] Mahmoud Assran, Mathilde Caron, Ishan Misra, Piotr Bojanowski, Florian Bordes, Pascal Vincent, Armand Joulin, Mike Rabbat, and Nicolas Ballas. Masked siamese networks for label-efficient learning. In *European Conference on Computer Vision*, pages 456–473, 2022. 3
- [3] Alberto Baldrati, Lorenzo Agnolucci, Marco Bertini, and Alberto Del Bimbo. Zero-shot composed image retrieval with textual inversion. In *Proceedings of the IEEE International Conference on Computer Vision*, pages 15338–15347, 2023. 2
- [4] Tom B. Brown, Benjamin Mann, Nick Ryder, Melanie Subbiah, Jared Kaplan, Prafulla Dhariwal, Arvind Neelakantan, Pranav Shyam, Girish Sastry, Amanda Askell, Sandhini Agarwal, Ariel Herbert-Voss, Gretchen Krueger, Tom Henighan, Rewon Child, Aditya Ramesh, Daniel M. Ziegler, Jeffrey Wu, Clemens Winter, Christopher Hesse, Mark Chen, Eric Sigler, Mateusz Litwin, Scott Gray, Benjamin Chess, Jack Clark, Christopher Berner, Sam McCandlish, Alec Radford, Ilya Sutskever, and Dario Amodei. Language models are few-shot learners. In *Advances in Neural Information Processing Systems*, 2020. 2
- [5] Mathilde Caron, Hugo Touvron, Ishan Misra, Hervé Jégou, Julien Mairal, Piotr Bojanowski, and Armand Joulin. Emerging properties in self-supervised vision transformers. In *Proceedings of the IEEE International Conference on Computer Vision*, pages 9630–9640, 2021. 5
- [6] Jia Deng, Wei Dong, Richard Socher, Li-Jia Li, Kai Li, and Li Fei-Fei. Imagenet: A large-scale hierarchical image database. In *Proceedings of the IEEE/CVF Conference on Computer Vision and Pattern Recognition*, pages 248–255, 2009. 2, 5
- [7] Jonathan Krause, Michael Stark, Jia Deng, and Li Fei-Fei. 3d object representations for fine-grained categorization. In *Proceedings of the IEEE International Conference on Computer Vision Workshops*, pages 554–561, 2013. 5
- [8] Alex Krizhevsky, Geoffrey Hinton, et al. Learning multiple layers of features from tiny images. *Technical Report TR-2009, University of Toronto, Toronto*, 2009. 5
- [9] A. Krizhevsky, I. Sutskever, and G. Hinton. Imagenet classification with deep convolutional neural networks. In *Advances in Neural Information Processing Systems*, pages 1097–1105, 2012. 3
- [10] Harold W. Kuhn. The hungarian method for the assignment problem. *Naval research logistics quarterly*, 2(1-2):83–97, 1955. 5
- [11] Yunfan Li, Peng Hu, Dezhong Peng, Jiancheng Lv, Jianping Fan, and Xi Peng. Image clustering with external guidance. In *International Conference on Machine Learning*, 2024. 2
- [12] Yuanpei Liu, Zhenqi He, and Kai Han. Hyperbolic category discovery. In *Proceedings of the IEEE/CVF Conference on Computer Vision and Pattern Recognition*, 2025. 2, 5
- [13] J. MacQueen. Some methods for classification and analysis of multivariate observations. In *Proceedings of the Fifth Berkeley Symposium on Mathematical Statistics and Probability*, pages 281–297, 1967. 2
- [14] Marco Mistretta, Alberto Baldrati, Lorenzo Agnolucci, Marco Bertini, and Andrew D. Bagdanov. Cross the gap: Exposing the intra-modal misalignment in clip via modality inversion. In *Proceedings of the International Conference on Learning Representations*, 2025. 4
- [15] Maria-Elena Nilsback and Andrew Zisserman. Automated flower classification over a large number of classes. In *Sixth Indian Conference on Computer Vision, Graphics & Image Processing*, pages 722–729, 2008. 5
- [16] Rabah Ouldnooghi, Chia-Wen Kuo, and Zsolt Kira. Clipgcd: Simple language guided generalized category discovery, 2023. 1, 2, 5
- [17] Omkar M Parkhi, Andrea Vedaldi, Andrew Zisserman, and C V Jawahar. Cats and dogs. In *Proceedings of the IEEE/CVF Conference on Computer Vision and Pattern Recognition*, pages 3498–3505. IEEE, 2012. 5
- [18] Alec Radford, Jong Wook Kim, Chris Hallacy, Aditya Ramesh, Gabriel Goh, Sandhini Agarwal, Girish Sastry, Amanda Askell, Pamela Mishkin, Jack Clark, Gretchen Krueger, and Ilya Sutskever. Learning transferable visual models from natural language supervision. In *International Conference on Machine Learning*, pages 8748–8763, 2021. 1, 4, 5, 13
- [19] Sarah Rastegar, Mohammadreza Salehi, Yuki M Asano, Hazel Doughty, and Cees GM Snoek. Selex: Self-expertise in fine-grained generalized category discovery. In *European Conference on Computer Vision*, pages 440–458, 2024. 2, 5
- [20] Walter J Scheirer, Anderson de Rezende Rocha, Archana Sapkota, and Terrance E Boulton. Toward open set recognition. *IEEE transactions on pattern analysis and machine intelligence*, 35(7):1757–1772, 2012. 1
- [21] Laurens Van der Maaten and Geoffrey Hinton. Visualizing data using t-sne. *Journal of machine learning research*, 9(11), 2008. 7
- [22] Sagar Vaze, Kai Hant, Andrea Vedaldi, and Andrew Zisserman. Generalized category discovery. In *Proceedings of the IEEE/CVF Conference on Computer Vision and Pattern Recognition*, pages 7482–7491, 2022. 1, 2, 5, 11
- [23] C. Wah, S. Branson, P. Welinder, P. Perona, and S. Belongie. The caltech-ucsd birds-200-2011 dataset. Technical Report CNS-TR-2011-001, California Institute of Technology, 2011. 5
- [24] Enguang Wang, Zhimao Peng, Zhengyuan Xie, Fei Yang, Xialei Liu, and Ming-Ming Cheng. Get: Unlocking the multi-modal potential of clip for generalized category discovery. In *Proceedings of the IEEE/CVF Conference on Computer Vision and Pattern Recognition*, pages 20296–20306, 2025. 1, 2, 3, 5, 12, 13
- [25] Hongjun Wang, Sagar Vaze, and Kai Han. Sptnet: An efficient alternative framework for generalized category discovery with spatial prompt tuning. In *International Conference on Learning Representations*, 2024. 5
- [26] Peng Wang, Huikang Liu, Druv Pai, Yaodong Yu, Zhihui Zhu, Qing Qu, and Yi Ma. A global geometric analysis of

- maximal coding rate reduction. In *International Conference on Machine Learning*, 2024. [4](#)
- [27] Xin Wen, Bingchen Zhao, and Xiaojuan Qi. Parametric classification for generalized category discovery: A baseline study. In *Proceedings of the IEEE International Conference on Computer Vision*, pages 16544–16554, 2023. [2](#), [3](#), [5](#)
- [28] Yaodong Yu, Kwan Ho Ryan Chan, Chong You, Chaobing Song, and Yi Ma. Learning diverse and discriminative representations via the principle of maximal coding rate reduction. In *Advances in Neural Information Processing Systems*, pages 9422–9434, 2020. [1](#), [4](#)
- [29] Beichen Zhang, Pan Zhang, Xiaoyi Dong, Yuhang Zang, and Jiaqi Wang. Long-clip: Unlocking the long-text capability of clip. In *European Conference on Computer Vision*, pages 310–325, 2024. [3](#)
- [30] Sheng Zhang, Salman Khan, Zhiqiang Shen, Muzammal Naseer, Guangyi Chen, and Fahad Shahbaz Khan. Prompt-cal: Contrastive affinity learning via auxiliary prompts for generalized novel category discovery. In *Proceedings of the IEEE/CVF Conference on Computer Vision and Pattern Recognition*, pages 3479–3488, 2023. [2](#), [5](#)
- [31] Bingchen Zhao, Xin Wen, and Kai Han. Learning semi-supervised gaussian mixture models for generalized category discovery. In *Proceedings of the IEEE International Conference on Computer Vision*, pages 16577–16587, 2023. [2](#), [5](#)
- [32] Haiyang Zheng, Nan Pu, Wenjing Li, Nicu Sebe, and Zhun Zhong. Textual knowledge matters: Cross-modality co-teaching for generalized visual class discovery. In *European Conference on Computer Vision*, pages 41–58, 2025. [1](#), [2](#), [3](#), [4](#), [5](#), [12](#), [14](#)

A. Experimental Details

A.1. Datasets

In Table A.1, we provide a statistical summarization of the eight generic and fine-grained datasets. Among these benchmarks, the generic datasets including CIFAR-10, CIFAR-100, ImageNet-100 and ImageNet-1k consist of categories of open-world, whereas the fine-grained benchmarks including CUB, Stanford Cars, Oxford Pets, and Flowers102 are largely domain-specific. Following the GCD protocol [22], we select the first half of classes as the known categories for each benchmark dataset, except for CIFAR-100, in which we select the first 80 classes as the known categories.

Table A.1. Statistics of the benchmark datasets.

Dataset	Labelled		Unlabelled	
	#Image	#Class	#Image	#Class
CIFAR10	12.5K	5	37.5K	10
CIFAR100	20.0K	80	30.0K	100
ImageNet-100	31.9K	50	95.3K	100
ImageNet-1K	321K	500	960K	1000
CUB	1.5K	100	4.5K	200
Stanford Cars	2.0K	98	6.1K	196
Oxford Pets	1.9K	19	5.5K	37
Flowers102	0.3K	51	0.8K	102

A.2. Experiments Settings

Network Architecture. In Figure A.1, we present a detailed overview of our proposed Retrieval-based Text Aggregation (RTA). In Table A.2, we present the learnable parameters of network architecture. The visual and textual branches share the same architecture. Specifically, when using CLIP-B/16 as the backbone, we fine-tune the last residual attention block (which includes the multi-head self-attention mechanism, feed-forward network, and layer normalization), along with the image and text projectors of CLIP. Additionally, the dual-branch classifiers are learned with the fine-tuning of CLIP jointly.

Data Preparation. For each mini-batch, we generate a set of text embeddings for query images by integrating four

Table A.2. Model architectures. “CLIP” denotes the learnable parameters in CLIP and “Cls” denotes the classifiers.

CLIP	Last residual attention block: $\mathbb{R}^{512} \rightarrow \mathbb{R}^{512}$
	Image/text projector: $\mathbb{R}^{512} \rightarrow \mathbb{R}^{512}$
Cls.	Linear projection: $\mathbb{R}^{512} \rightarrow \mathbb{R}^K$
	Softmax function

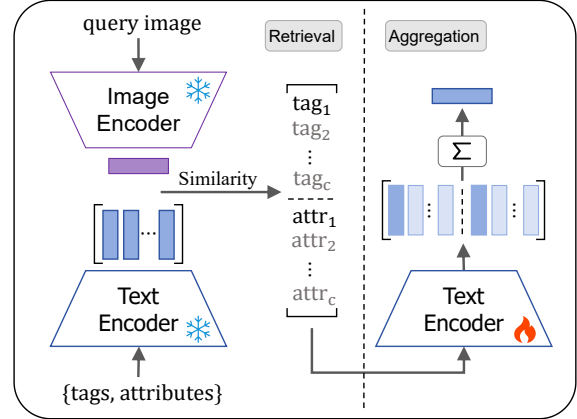


Figure A.1. An overview of Retrieval-based Text Aggregation (RTA).

Table A.3. Python code for the image augmentation.

```

from torchvision.transforms import *

Compose ([
    RandomResizedCrop(32, BILINEAR)
    RandomHorizontalFlip(p=0.5),
    ColorJitter()
    ToTensor(),
    Normalize([0.485, 0.456, 0.406],
              [0.229, 0.224, 0.225])
])

```

Table A.4. Pseudo-code for the text augmentation.

```

Input: text
For each word in text:
    If len(word) ≥ 3:
        index ← random(1, len(word)-2)
        action ← random({replace, delete, add, none})
        Case action:
            replace: word ← replace random char at index
            delete: word ← remove char at index
            add: word ← insert random char at index
            none: continue
Output: augmented text

```

similar tags and four similar attributes through the proposed RTA strategy by using the encoders of CLIP-H/14 for all test datasets. Then, both images and text are augmented into two views, and the augmentation strategies are the same across datasets, as detailed in Tables A.3 and A.4. The embeddings of augmented images and text are used for representation learning.

Training Settings. We use Stochastic Gradient Descent (SGD) with the momentum of 0.9, the weight decay of 1×10^{-4} , and using cosine annealing learning rate decay for the training process. We train the model for 200 epochs and set the batch size to 128. The random seeds for the

Table A.5. The mean \pm std ACC (%) of TextGCD, GET and our approach on generic datasets.

Method	CIFAR-10			CIFAR-100			ImageNet-100			ImageNet-1k		
	All	Old	New	All	Old	New	All	Old	New	All	Old	New
TextGCD	98.2 \pm 0.0	98.0 \pm 0.2	98.6 \pm 0.1	85.7 \pm 0.9	86.3 \pm 0.6	84.6 \pm 2.2	88.0 \pm 0.6	92.4 \pm 0.9	85.2 \pm 1.2	64.8 \pm 0.2	77.8 \pm 0.5	58.3 \pm 0.4
GET	97.2 \pm 0.1	94.6 \pm 0.1	98.5 \pm 0.1	82.1 \pm 0.4	85.5 \pm 0.5	75.5 \pm 0.5	91.7 \pm 0.3	95.7 \pm 0.0	89.7 \pm 0.4	62.4 \pm 0.0	74.0 \pm 0.2	56.6 \pm 0.1
Ours	98.5 \pm 0.2	98.3 \pm 0.2	98.6 \pm 0.3	86.4 \pm 0.5	86.2 \pm 0.6	86.9 \pm 1.6	92.1 \pm 0.3	96.0 \pm 0.6	90.2 \pm 0.8	66.7 \pm 0.1	77.3 \pm 0.3	61.1 \pm 0.2

Table A.6. The mean \pm std ACC (%) of TextGCD, GET and our approach on fine-grained datasets.

Method	CUB			Stanford Cars			Oxford Pets			Flowers102		
	All	Old	New	All	Old	New	All	Old	New	All	Old	New
TextGCD	76.6 \pm 0.6	80.6 \pm 2.0	74.7 \pm 1.7	86.1 \pm 0.9	91.8 \pm 0.4	83.9 \pm 1.3	93.7 \pm 0.6	93.2 \pm 1.1	94.0 \pm 0.9	87.2 \pm 2.3	90.7 \pm 1.3	85.4 \pm 3.8
GET	77.0 \pm 0.5	78.1 \pm 1.6	76.4 \pm 1.2	78.5 \pm 1.3	86.8 \pm 1.5	74.5 \pm 2.2	91.1 \pm 1.0	89.7 \pm 1.6	92.4 \pm 1.2	85.5 \pm 0.5	90.8 \pm 1.5	81.3 \pm 1.7
Ours	78.3 \pm 0.8	78.5 \pm 1.2	78.2 \pm 0.9	89.2 \pm 0.3	93.1 \pm 0.9	87.3 \pm 0.2	95.7 \pm 0.2	95.1 \pm 0.5	96.0 \pm 0.4	93.5 \pm 0.4	93.3 \pm 0.8	93.9 \pm 1.0

three trials are set to $\{0, 1, 2\}$. For representation learning, the initial learning rate for CLIP is set to 0.001, and our proposed objective $\mathcal{L}_{\text{SSR}^2}$ does not need an extra balancing hyper-parameter, except for ϵ which is set as 0.5. The initial learning rate for the two classifiers is set to 0.1, the epochs for warm-up stage is set to 10, and 60% of pseudo-labels of each categories are selected for co-teaching. We use the same setting for all test datasets. All experiments are conducted on a single NVIDIA GeForce RTX3090 GPU.

B. More Experiments

B.1. Evaluation on Model Stability

In Tables A.5 and A.6, we report the mean accuracy with standard deviation (\pm std) over 3 trials across the test datasets, and compare to the multi-modal counterparts TextGCD [32] and GET [24]. As can be seen, the performance of our proposed SSR^2 -GCD is relatively stable.

B.2. Effect of Retrieval-based Text Aggregation

Table B.7. The number of identical tags between the candidate pool and the unknown categories in four benchmark datasets.

Dataset	# Unknown categories	# Removed tags
CUB-200	100	90
Stanford Cars	98	83
Flowers102	51	43
Oxford Pets	19	17

In Table B.7, we report the results of our SSR^2 -GCD compared to TextGCD [32] when removing the prompts of the *unknown* categories for each dataset from the candidate pool, since that the prompts in candidate pool may semantically identical to the unknown categories. As can be seen

in Table B.8, though the performance of both methods is slightly dropped, our SSR^2 -GCD is still leading.

Table B.8. Effect of retrieval-based methods with or without (w/o) prompts from unknown categories on four test datasets. ACC (%) on “All” categories is reported.

Datasets	CUB	Cars	Pets	Flowers
TextGCD [32]	76.6	86.1	93.7	87.2
TextGCD (w/o)	75.7	85.5	91.5	84.0
SSR^2 -GCD (w/o)	77.6	88.1	94.0	91.6

B.3. Evaluation on Modality Alignments for Representation Learning

Evaluation on More Inter-Modal Alignment Methods.

To further evaluate the necessity of inter-modal alignment, we report the performance of using different inter-modal alignment loss for training our SSR^2 -GCD. Specifically, we introduce a Cross-modal Instance Consistency Objective (CICO) which is proposed in GET [24] as an inter-modal alignment constraint. CICO is defined as follows:

$$\mathcal{L}_{\text{CICO}} = \frac{1}{2|B|} \sum_{i \in B} (D_{\text{KL}}(s_i^T \| s_i^I) + D_{\text{KL}}(s_i^I \| s_i^T)), \quad (13)$$

where D_{KL} is the Kullback-Leibler divergence, B denotes the mini-batch data, $s_i^I = \text{softmax}(z_i^I \mathcal{A}^I)$ and $s_i^T = \text{softmax}(z_i^T \mathcal{A}^T)$ measure the similarity between the i -th image/text embeddings and prototypes, and \mathcal{A}^I and \mathcal{A}^T are the prototypes determined by the labeled anchors for each modality.

In Table B.9, we report the performance of using $\mathcal{L}_{\text{CICO}}$ and its combination with the intra-modal alignment losses for representation learning, in which the results are marked in gray. As can be seen that, both inter-modal alignment

losses $\mathcal{L}_{\text{CLIP}}$ and $\mathcal{L}_{\text{CICO}}$ fail to bring performance improvements when combining with the intra-modal alignment loss. This further confirms that performing extra inter-modal alignment is not necessary.

Table B.9. Evaluation of different representation learning methods. Average ACC (%) on “All” categories is reported. “N/A” denotes using a frozen CLIP.

Rep. Losses	Inter	Intra	C-10	C-100	CUB	Cars	Pets	Flowers
N/A	×	×	97.9	84.1	74.5	86.0	91.9	87.4
$\mathcal{L}_{\text{CLIP}}$	✓	×	98.3	86.0	76.6	86.7	93.9	89.7
$\mathcal{L}_{\text{CICO}}$	✓	×	98.0	85.0	76.4	86.1	94.9	87.2
\mathcal{L}_{con}	×	✓	98.4	86.7	77.5	87.9	94.9	91.8
$\mathcal{L}_{\text{SSR}^2}$	×	✓	98.5	86.4	78.3	89.2	95.7	93.5
$\mathcal{L}_{\text{CLIP}}+\mathcal{L}_{\text{con}}$	✓	✓	98.2	86.3	78.0	86.7	95.0	90.9
$\mathcal{L}_{\text{CICO}}+\mathcal{L}_{\text{con}}$	✓	✓	98.4	85.9	76.8	87.0	94.4	88.6
$\mathcal{L}_{\text{CLIP}}+\mathcal{L}_{\text{SSR}^2}$	✓	✓	98.3	86.1	77.2	88.1	95.0	92.9
$\mathcal{L}_{\text{CICO}}+\mathcal{L}_{\text{SSR}^2}$	✓	✓	98.3	86.1	76.7	87.5	95.5	92.1

To further verify that extra inter-modal alignment may be not necessary, and jointly optimizing inter-modal alignment and intra-modal alignment significantly impairs feature learning, we validate the role of inter-modal alignment under different text prompt qualities (i.e., which associate with different noise levels). Specifically, in the RTA strategy, we employ three frozen CLIP models [18]—namely CLIP-H/14, CLIP-L/14, and CLIP-B/16—to perform prompt searching, in order to evaluate how inter-modal alignment affects model performance under varying prompt qualities. The results in Table B.10 show that, on Stanford Cars and Flowers102, introducing an extra $\mathcal{L}_{\text{CLIP}}$ loss for joint training with $\mathcal{L}_{\text{SSR}^2}$ consistently degrades clustering performance at all levels of prompt quality.

Evaluation on Uni-Modal Representation Learning. To evaluate its effectiveness of the proposed $\mathcal{L}_{\text{SSR}^2}$ as an intra-modal alignment loss, we apply $\mathcal{L}_{\text{SSR}^2}$ to uni-modal GCD counterparts and report their clustering performance. Specifically, for GCD and SimGCD frameworks, we keep their pre-trained models and clustering algorithms unchanged, but replace the supervised and unsupervised contrastive loss \mathcal{L}_{con} with our proposed $\mathcal{L}_{\text{SSR}^2}$. As can be read from Table B.11 that, using our $\mathcal{L}_{\text{SSR}^2}$ for representation learning achieves improvements on most cases.

Evaluation on Effect of Inter-Modal Alignment against Intra-Modal Alignment. To evaluate the effect of performing inter-modal alignment against intra-modal alignment, we combine our proposed intra-modal alignment loss $\mathcal{L}_{\text{SSR}^2}$ with the inter-modal alignment loss $\mathcal{L}_{\text{CLIP}}$ by introducing a tradeoff parameter $\nu > 0$, i.e.,

$$\mathcal{L}_{\text{SSR}^2} + \nu \cdot \mathcal{L}_{\text{CLIP}},$$

where using a larger ν means to emphasizing more on the inter-modal alignment. In Figure B.2, we report the ac-

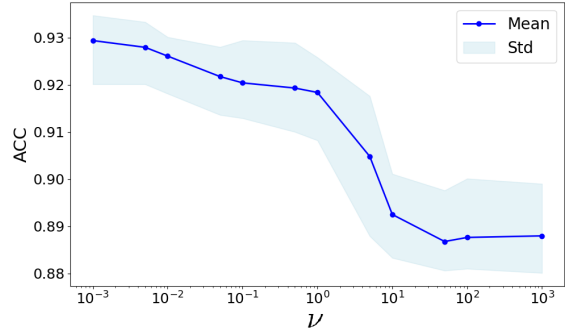


Figure B.2. Mean accuracy with standard deviation over 3 trials of “All” categories with varying penalty weight ν on Flowers102.

curacy as a function with respect to a varying ν on Flowers102. Existing multi-modal GCD frameworks, such as GET [24], assume that enforcing an inter-modal alignment does not affect that of intra-modal alignment, and simply treat these two alignments in representation learning as independent and equally important. However, our experiments reveal here that the more emphasizing upon inter-modal alignment (i.e., via $\mathcal{L}_{\text{CLIP}}$ with a larger ν), rather than upon the intra-modality alignment (i.e., via $\mathcal{L}_{\text{SSR}^2}$), the lower the clustering accuracy is.

More Results on Consistency Measure ρ . Recall that we define a consistency measure ρ in Eq.(12) to quantify the intra-modal consistency of the embeddings to explain why extra inter-modal alignment could be unnecessary. Here, we additionally report the consistency measure ρ when training via inter-modal alignment loss (i.e., $\mathcal{L}_{\text{CLIP}}$), intra-modal alignment losses (i.e., \mathcal{L}_{con}) and their combinations (i.e., $\mathcal{L}_{\text{con}} + \mathcal{L}_{\text{CLIP}}$) on Stanford Cars. We display the experimental results in Figure B.3. As can be seen that, the inter-modal alignment also damages the learning of other intra-modal losses such as the widely adopted supervised and unsupervised contrastive loss \mathcal{L}_{con} .

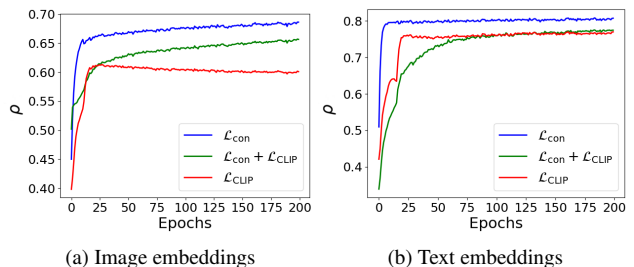


Figure B.3. Consistency measure ρ as a function of training epoch under different losses on Stanford Cars.

Table B.10. Accuracy comparison of models using different feature learning methods under various text prompt qualities. Δ denotes the accuracy difference before and after adding the inter-modal alignment loss $\mathcal{L}_{\text{CLIP}}$, and “ \downarrow ” indicates accuracy drop.

Text retrieval models	Prompt qualities	Stanford Cars			Flowers102		
		$\mathcal{L}_{\text{SSR}^2}$	$\mathcal{L}_{\text{SSR}^2} + \mathcal{L}_{\text{CLIP}}$	Δ	$\mathcal{L}_{\text{SSR}^2}$	$\mathcal{L}_{\text{SSR}^2} + \mathcal{L}_{\text{CLIP}}$	Δ
CLIP-H/14	High	89.2	88.1	1.1 \downarrow	93.5	92.9	0.6 \downarrow
CLIP-L/14	Medium	87.5	86.1	1.4 \downarrow	92.4	91.8	0.6 \downarrow
CLIP-B/16	Low	85.2	84.0	1.2 \downarrow	90.1	89.8	0.3 \downarrow

Table B.11. Comparison to uni-modal counterparts. ACC (%) on generic and fine-grained datasets is reported.

Method	CIFAR-10			CIFAR-100			CUB			Stanford Cars			Oxford Pets			Flowers102		
	All	Old	New	All	Old	New	All	Old	New	All	Old	New	All	Old	New	All	Old	New
GCD	91.5	97.9	88.2	73.0	76.2	66.5	51.3	56.6	48.7	39.0	57.6	29.9	80.2	85.1	77.6	74.4	74.9	74.1
GCD+SSR ²	92.5	96.4	91.6	73.9	79.0	63.2	51.9	55.0	47.1	47.9	56.1	47.3	83.6	87.7	79.8	80.0	83.3	78.5
SimGCD	97.1	95.1	98.1	80.1	81.2	77.8	60.3	65.6	57.7	53.8	71.9	45.0	87.7	85.9	88.6	71.3	80.9	66.5
SimGCD+SSR ²	97.6	97.5	97.7	81.1	82.5	78.9	60.8	64.7	59.0	57.1	66.8	53.9	90.0	89.8	91.2	81.6	83.5	80.1

B.4. Evaluation on Parameter ϵ in SSR²

To evaluate the impact of using different hyper-parameters ϵ in our SSR²-GCD, we keep all other hyper-parameters fixed, and conduct experiments under different parameter ϵ on six benchmark datasets, i.e., CIFAR-10, CIFAR-100, CUB, Stanford Cars, Oxford Pets and Flowers102. Experimental results are reported in Figure B.4. As can be seen, our SSR²-GCD framework is not sensitive to ϵ and achieves the best performance when ϵ is in the range of [0.2, 0.5].

B.5. Visualization

In Figure B.5, we use *t*-SNE to visualize the image embeddings and text embeddings of our SSR²-GCD framework using different representation learning methods on Oxford Pet, which comprises 12 categories of cats and 25 categories of dogs. As can be seen, the image embeddings produced by using the frozen CLIP image encoder exhibit a distribution that can only be roughly partitioned into two classes (i.e., “cat” and “dog”). In contrast, thanks to our proposed RTA strategy, the distribution of text embeddings produced by using the frozen CLIP text encoder assisted with our RTA exhibits significant discriminability. Meanwhile, training via $\mathcal{L}_{\text{CLIP}}$ fails to learn well-aligned intra-modal relationships (See, e.g., Figure B.5a and Figure B.5b for comparison). In contrast, our SSR²-GCD learns discriminative and well-balanced representations for both modalities.

B.6. Learning Curves

We compute the clustering accuracy (ACC) as a function of epoch during training period, and display the ACC curves on different datasets in Figure B.6. We can observe that our SSR²-GCD converges and achieves stable clustering performance on “All” categories roughly within 50 epochs.

Table B.12. Running time and memory costs on Flowers102. “ \dagger ” denotes to use the method in TextGCD [32] to produce text features.

Methods	Running Time (sec/iter)			Memory (MB)	
	Forward	Backward	Overall	w/o RTA [†]	w/ RTA
TextGCD [32]	0.34	6.7×10^{-3}	0.69	7,622	-
SSR ² -GCD	0.57	7.5×10^{-2}	0.92	8,035	11,080

B.7. Computation Time and Memory Costs

We report the running time and memory costs on Flowers102 of our SSR²-GCD in Table B.12. Note that the coding rate term $\log \det(\cdot)$ is cheap to handle because its scale is kept to $\min\{|B|, d\}$ due to the fact that $\log \det(\mathbf{I} + \mathbf{Z}\mathbf{Z}^\top) = \log \det(\mathbf{I} + \mathbf{Z}^\top\mathbf{Z})$. Comparing to TextGCD [32], the increased costs of our SSR²-GCD is due to the RTA step in forward pass.

B.8. Performance Evaluation on Using Varying K

To evaluate the sensitivity of our SSR²-GCD to the category number K , we change the output dimensions of the classifiers d_{cls} to deviate from the total number of categories K , and report the clustering accuracy (ACC), Normalized Mutual Information (NMI) and Adjusted Rand Index (ARI) of our SSR²-GCD with varying d_{cls} on Flowers102 in Figure B.7. As can be observed that, our SSR²-GCD achieves relatively high clustering performance when $d_{\text{cls}} \approx K$ (e.g., $d_{\text{cls}} \in \{100, 102, 104\}$). Specifically, our SSR²-GCD is sensitive to under-specification, where all metrics degrade sharply when $d_{\text{cls}} < K$; whereas our SSR²-GCD exhibits good robustness to over-specification, where all metrics degrades slightly. We notice of that NMI remains nearly unchanged as d_{cls} increases beyond K .

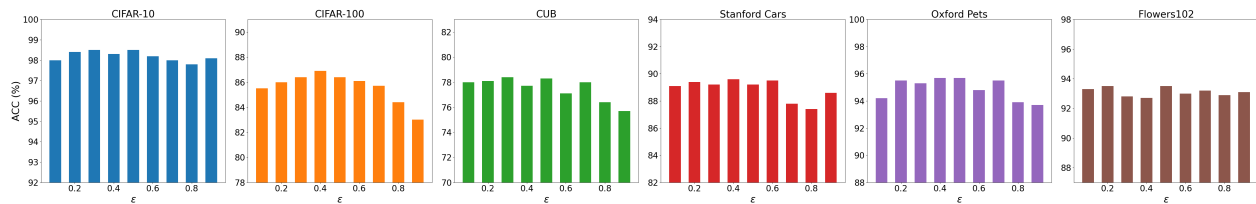


Figure B.4. ACC (%) with varying ϵ in SSR^2 across six benchmark datasets.

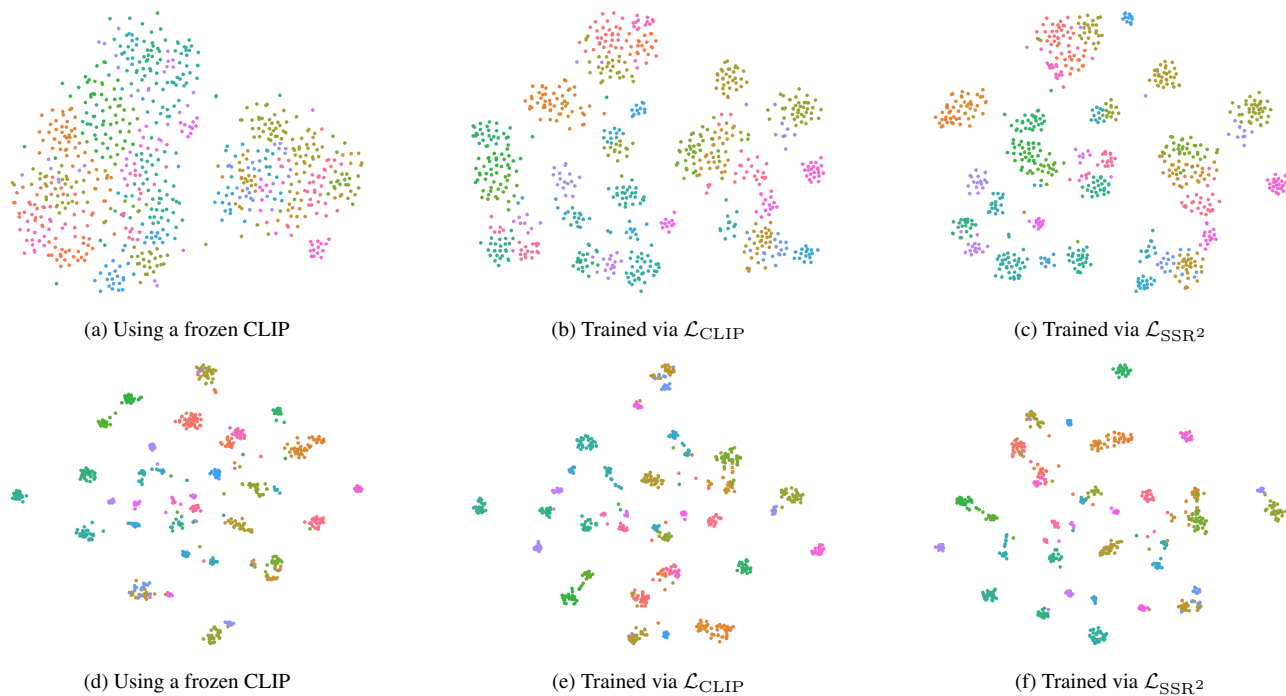


Figure B.5. Visualization of image embeddings (**top**) and text embeddings (**bottom**) on Oxford Pets.

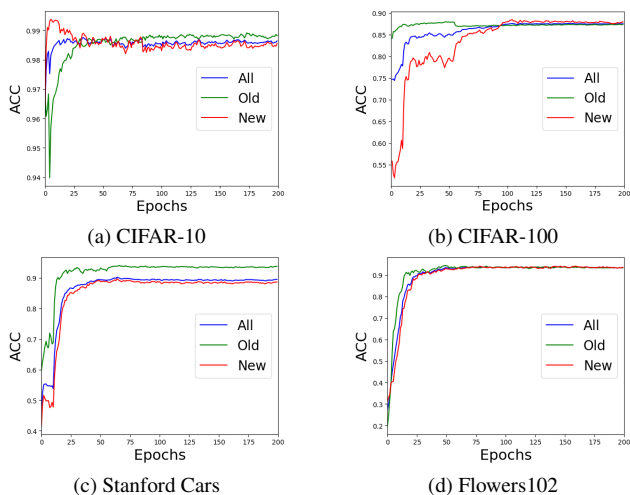


Figure B.6. ACC curves on benchmark datasets.

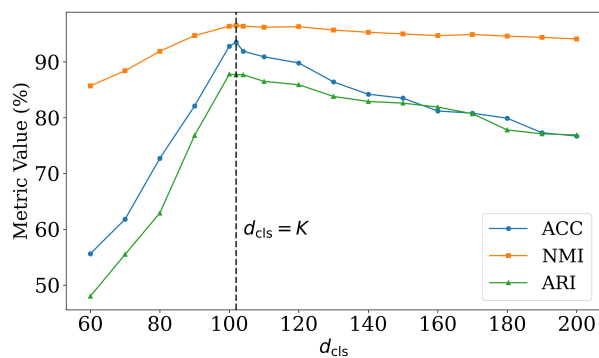


Figure B.7. Evaluation on Clustering performance ACC, NMI and ARI of our SSR^2 -GCD with varying d_{cls} on Flowers102.